Applied Physics Letters

RESEARCH ARTICLE | MAY 23 2023

Ion-implanted triple-zone graded junction termination extension for vertical GaN p-n diodes

Yu Duan; Jingshan Wang; Zhongtao Zhu; ... et. al

Appl. Phys. Lett. 122, 212104 (2023)
https://doi.org/10.1063/5.0144898

AIP Publishing

Applied Physics Letters ARTICLE pubs.aip.org/aip/apl

Ion-implanted triple-zone graded junction termination extension for vertical GaN p-n diodes

Cite as: Appl. Phys. Lett. **122**, 212104 (2023); doi: 10.1063/5.0144898
Submitted: 1 February 2023 · Accepted: 11 May 2023 ·
Published Online: 23 May 2023

View Online Export Citation CrossMark

Yu Duan,[1] Jingshan Wang,[2] Zhongtao Zhu,[1] Guanxi Piao,[3] Kazutada Ikenaga,[3] Hiroki Tokunaga,[3] Shuuichi Koseki,[3] Mayank Bulsara,[4] and Patrick Fay[1,a)]

AFFILIATIONS

[1]University of Notre Dame, Notre Dame, Indiana 46556, USA
[2]Micron Technology, Inc., Boise, Idaho 83707, USA
[3]Taiyo Nippon Sanso, Innovation Division, Tokyo, Japan
[4]Matheson Tri-Gas, Inc., Irving, Texas 75039, USA

[a)]Author to whom correspondence should be addressed: pfay@nd.edu

ABSTRACT

We demonstrate an ion-implanted triple-zone junction termination extension (JTE) for vertical GaN p-n diodes. Due to the spatial distribution of fixed charge in the triple-zone JTE structure, the peak electric fields at the contact metal edge and at the edge of the JTE are significantly reduced compared to conventional approaches. The forward and reverse characteristics of diodes with conventional single-zone JTE and the triple-zone JTE explored here have been studied and compared experimentally. GaN p-n diodes fabricated using the triple-zone JTE obtain an experimentally measured maximum breakdown voltage of 1.27 kV, appreciably higher than the 1.01 kV achieved using the single-zone JTE structure. The triple-zone JTE design also provides a wider window for fabrication processing and epitaxial wafer growth to achieve the high breakdown voltage compared to single-zone designs. The triple-zone JTE is promising for cost-effective fabrication of GaN power electronics.

GaN is among the most promising candidates for use in high frequency power electronic devices due to its excellent material properties, including large bandgap, high breakdown electric field, high thermal conductivity, high electron mobility, and high saturation velocity.[1] These lead to the potential for realizing power devices with lower on-resistance, higher breakdown, and lower power conversion loss during high frequency operation compared to Si and SiC.[2,3] Despite these intrinsic material-level advantages, the high dislocation density in GaN grown on non-native substrates, such as sapphire, Si, and SiC, can limit device performance.[4] Recently, however, the improved quality of native GaN substrates with low defect densities ($<10^6\,cm^{-2}$) has resulted in emerging high breakdown and low on-resistance GaN power diodes.[5–19]

An additional factor that can compromise the performance of GaN devices is the termination of the electric fields around the perimeter of the device. Electric field management at the periphery of the device is required, especially for large voltage blocking applications, since unsatisfactory edge terminations (ETs) lead to electric field crowding at the device edge and early onset of breakdown.[20] Junction termination extension (JTE) structures are widely used in Si and SiC power devices,[21–23] but many of these approaches are more difficult to realize in GaN because of inherent challenges associated with p-type doping in III-nitride materials.[24] As alternatives to doping-based ET, a number of edge termination designs have been studied to alleviate the electric field crowding in vertical GaN diodes. These include the use of anode-connected field plates (FPs),[6–8] surface plasma treatments to compensate doping,[9–11] vertical and/or stepped mesa etching[12–14] as well as negative beveled-mesas[15,16] to control the geometry and spread the field, and guard rings (GRs).[17–19] While these approaches can be effective, each has drawbacks that may limit adoption in practice, including fabrication complexity and cost, sensitivity to the details of fabrication (e.g., the need for low-damage etched sidewalls with precise angles, the need for etched rings or steps with precisely controlled depth, or the need for very precise doping compensation profiles), or reliability and/or stability concerns. Thus, it remains a significant challenge to realize reliable and repeatable devices due to fabrication and

wafer variation. Another alternative to conventional doping-based termination is to use nitrogen implantation to selectively compensate dopants incorporated during growth to form a compensation-based JTE.[25,26] This structure has been demonstrated experimentally to spread the electric field laterally away from the edge of the anode metallization and enhance breakdown voltage,[25,26] without relying on precise etching profiles or depth control. However, in this bilayer design, the breakdown voltage is very sensitive to the exact JTE thickness and charge concentration. Any variations in the epitaxial layer thickness or doping profile also affect the doping concentration profile within the edge termination.[27] In this paper, we demonstrate through simulation and experiment a triple-zone JTE structure that more effectively distributes the electric field in vertical p-n diodes. The measurement results show that the proposed triple-zone structure provides higher breakdown voltage and extends the fabrication process window of the edge termination, while also tolerating epitaxial growth variations (in terms of deviation from the targeted values for p-GaN doping and thickness). This simple fabrication process flow makes use of well-established and low-cost ion implantation processing without the need for precision etching or concern about residual etch damage.

Schematic cross-sectional illustrations of the conventional single-zone and the proposed triple-zone JTE structures evaluated here are shown in Fig. 1. The epilayers were grown on 2-in. diameter n-GaN free standing substrates by metalorganic chemical vapor deposition (MOCVD) at Taiyo Nippon Sanso Corporation. From the bottom to the top, the epitaxial structure consists of a 1 μm n^+ GaN buffer layer with Si concentration of 3×10^{18} cm^{-3}, a 10 μm thick n^- GaN drift layer doped with Si at a concentration of 1×10^{16} cm^{-3}, a 300 nm thick p^+ GaN layer, doped with a Mg concentration of 1×10^{19} cm^{-3}, and a 100 nm thick heavily doped p^{++} GaN cap with a Mg concentration of 1×10^{20} cm^{-3} to facilitate low resistance Ohmic contacts.

Fabrication of the vertical GaN diodes started with activation of the Mg acceptors by thermal annealing of the as-grown epitaxial wafers at 850 °C in a nitrogen ambient for 15 min. The top-side anode Ohmic contact was formed by photolithography and evaporated Ni/Au (30/100 nm), followed by an anneal in air at 525 °C for 10 min. A two-step surface pretreatment before evaporation was used to enhance Ohmic contact.[28] The anode metal contact is circular to avoid field concentration from corners. The bottom Ohmic contact was formed by evaporating Ti/Al/Ni/Au (30/100/50/100 nm) on the backside of the GaN substrates, and subsequently annealed at 800 °C in a nitrogen ambient for 1 min. Devices were isolated by etching a 160 nm deep, 20 μm wide ring into the p-GaN layer at a distance of 60 μm from the edge of the p-contact by BCl_3/Cl_2-based inductively coupled plasma reactive ion etching (ICP-RIE). After etching, the edge termination structure was implemented using a series of photolithography and nitrogen implant steps as will be described in detail below. Finally, the device was passivated using 250 nm of sputtered SiN_x.

A series of nitrogen (N^{14}) triple implants was performed to form the edge termination structures. The defect concentration depth profiles arising from the implants were calculated by the Stopping and Range of Ions in Matter (SRIM) software;[29] Fig. 2(a) shows an example of a representative simulation result. Since N cannot dope GaN substitutionally, the implant-induced defects generate deep levels that compensate the Mg-doped p-GaN. By using three implants of different energy, the superposition of the three implants results in an approximately constant defect concentration ($\sim 2 \times 10^{20}$ cm^{-3}) to a depth of ~250 nm, followed by a gradually deceasing tail at greater depths, as shown in Fig. 2(a). This implant profile fully compensates the p-type regions above the doping concentration [shown as dashed blue line in Fig. 2(a)] but only partially compensates the lower portion of the p-GaN region (shown as the region between the orange and green vertical dashed lines; for the structure reported here, the metallurgical junction is 400 nm from the surface). Such an implant forms the bilayer structure reported previously.[27] This bilayer's lateral extent is limited by the isolation ring that is etched before implant.

As noted previously, a single-zone JTE is very sensitive to the thickness of the partially compensated layer p^- layer. This thickness, denoted as t_p in Fig. 2(a), can be changed by adjusting the highest ion-implantation energy, with higher implant energies resulting in smaller t_p values. For the conventional single-zone design, the p^- layer thickness (t_p) is constant over the full width of the JTE structure (i.e., from the edge of the anode metallization to the inner edge of the etched isolation ring; 60 μm for the devices reported here). To realize the triple-zone design, the t_p thickness was decreased in a staircase fashion with distance from the anode contact. This was achieved by using a series of photolithography steps to expose each zone, which was subsequently implanted. The innermost zone was implanted using the same recipe as the single-zone design. The outer zones had a thinner t_p value, which was achieved by using a higher energy for the high-energy implant step, increasing by 5 keV for each zone, as illustrated in Fig. 2(b). This concept is shown schematically in Fig. 2(c), superimposed on an optical micrograph of a typical fabricated device. For the triple-zone devices, the width of each zone is 20 μm, and the total length for the triple-zone case is 60 μm.

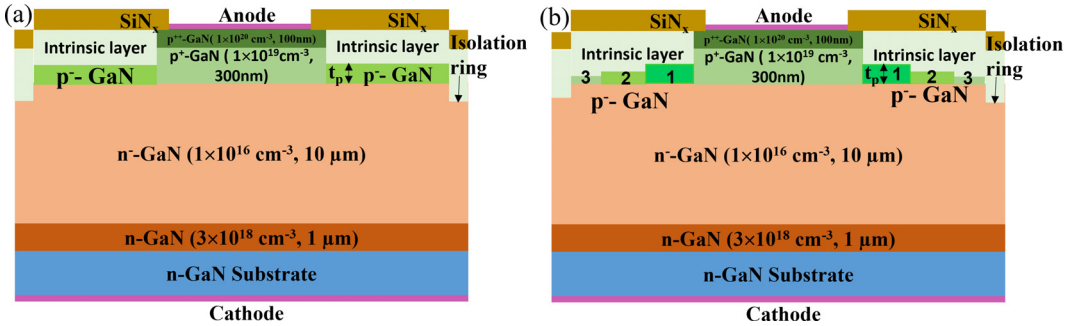

FIG. 1. Cross-sectional schematic of the (a) single-zone and (b) triple-zone JTE GaN vertical p-n diodes.

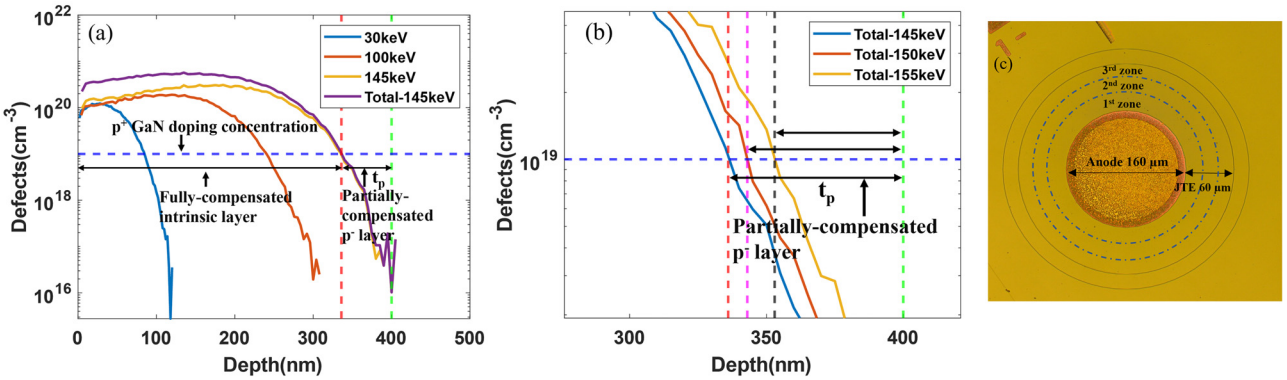

FIG. 2. (a) SRIM simulation of defect density vs depth for N^{14} implants with different ion energies, and the total superposition of the triple implants. (b) SRIM simulation showing that increasing the highest-energy implant reduces t_p. (c) A top view of a fabricated p-n diode, with the implant zones shown for illustration. The single-zone and triple-zone devices look the same under a microscope.

Capacitance-voltage (C-V) measurements were performed to analyze the net doping concentration of the n-GaN drift layer; an average net carrier concentration N_D-N_A of the n-GaN drift region is $9.6 \times 10^{15}\,cm^{-3}$, in good agreement with the intended doping density target of $1 \times 10^{16}\,cm^{-3}$.

In order to visualize the impact of the JTE design on internal field distributions within the fabricated devices, self-consistent drift-diffusion simulations of the two JTE structures were performed using Synopsys Sentaurus TCAD.[30] The numerically simulated electric field distributions inside the diode with single-zone JTE for the optimum choice of t_p are shown in Fig. 3(a) at an applied voltage of 1.6 kV. The electric field profile along the metallurgical p-n junction [dashed line in Fig. 3(a)] is extracted and shown in Fig. 3(b). For the single-zone case, the electric field shows two sharp peaks: one at the edge of the main junction (point A), and the other at the outer edge of the JTE (point B). The fact that these two peaks are nearly the same magnitude indicates that the optimum t_p for single-zone structure has been achieved, since uneven magnitudes would lead to premature breakdown at one or the other location.[25,26]

Even though this single-zone JTE does reduce the field crowding effect to some extent, the peaky electric field profile is not optimal for maximizing breakdown voltage. In addition, the breakdown voltage of this design is very sensitive to the JTE thickness, with a window of allowable t_p values smaller than 10 nm.[25,26] To address this shortcoming, a JTE design with a larger density of fixed charges in the JTE near the main junction and lower density of charges at the outermost region is advantageous. Figure 4(a) shows a graded profile for the JTE charge as a function of distance across the JTE. This graded profile results in a gradual decrease in charge density with increasing radius in the termination and, consequently, a gradual and smooth field distribution across the termination region. This graded profile was found to give excellent breakdown characteristics in simulation. In practice, such a continuously graded profile is difficult to achieve. Instead, we approximated this with a triple-zone structure by selecting t_p thicknesses decreasing in a staircase fashion with distance from the anode contact, as shown in Fig. 4(a). The resulting electric field profile inside the structure is simulated and shown in Fig. 4(b). The electric field profile along the metallurgical p-n junction [dashed line in Fig. 4(b)] is extracted and compared with a single-zone structure in Fig. 4(c). For the triple-zone JTE design, the electric field gradually decreases along the edge termination and effectively alleviates the peak electric field at the edge of the electrode and JTE due to the effective decreasing lateral charge.

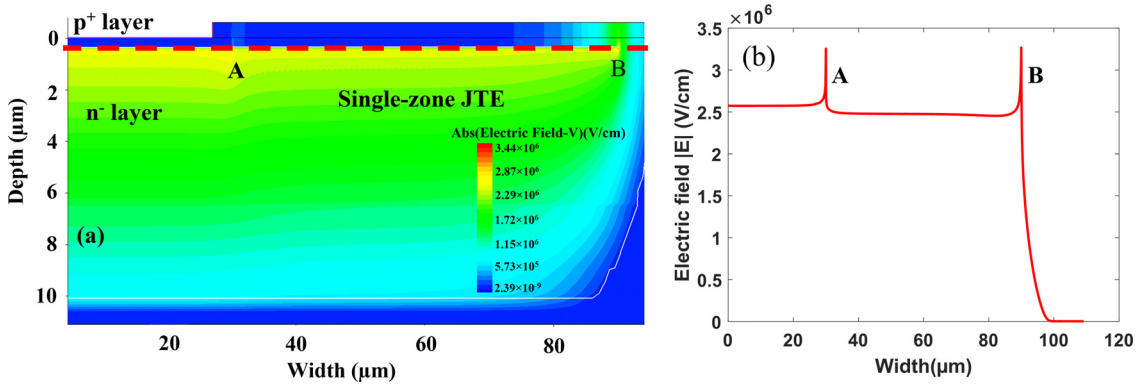

FIG. 3. (a) TCAD simulation of the electric field distribution for a diode with optimized single-zone JTE. (b) Electric field magnitude along the metallurgical junction of the diode [cut shown as dashed line in (a)].

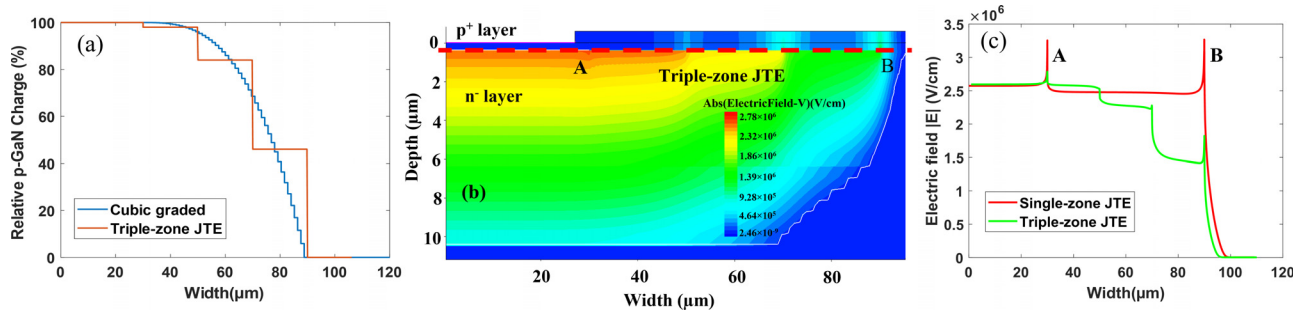

FIG. 4. (a) Relative p-GaN charge percentage horizontally along JTE. (b) TCAD simulation of electric field distribution for triple-zone JTE structure. (c) Electric field distribution along the interface of p-n junction as indicated by dashed line for single-zone [Fig. 3(a)] and triple-zone (b) JTE structures.

Devices with single- and triple-zone JTE designs were fabricated as described above. The measured forward-bias IV characteristics of diodes with each type of edge termination are shown in Figs. 5(a) and 5(b). The current density was calculated using the anode metal area. Devices with anode diameters from 70 to 550 μm were tested. In forward bias, the current density was found to be modestly higher for the smaller-area devices, and this dependence was more significant for the single-zone design than the triple-zone structure, indicative of increased defect-mediated leakage current. Low-bias ideality factors of 2 were measured for the single-zone and triple-zone JTE structures, respectively, indicating Shockley–Read–Hall (SRH) recombination. The ideality factor dropped to 1.4 and 1.6 at 2.8 V for the single-zone and triple-zone JTE structures, respectively, indicating that diffusion-dominated transport could be achieved with both structures. Above this, the ideality factor increases due to series resistance. The specific on resistance (R_{on}) for diodes with diameter 70 μm at 5 V is comparable in the range of 0.6 to 0.8 mΩ cm^2 for both designs.

Measured reverse-bias IV characteristics of diodes with different values of t_p for single-zone and triple-zone JTE structures are shown in Figs. 6(a) and 6(b), respectively. The reverse-bias characteristics are measured in Fluorinert to avoid breakdown in air or at the surface of the device. The t_p variations lead to different electric field profiles within the device and, hence, different breakdown voltages (V_{br}). If the t_p is too small (i.e., the implant is too deep), the JTE will deplete at a much lower voltage and result in premature breakdown at contact edge. As the t_p becomes thicker, the breakdown voltage increases due to the JTE depleting at a larger voltage and the broader spread of electric field. However, too thick t_p will cause breakdown to occur at the outermost JTE edge at low applied voltage.[25,26] For single zone devices, a maximum breakdown voltage of 1.01 kV is measured at t_p equal to 63 nm. In contrast, the highest breakdown voltage achieved by triple-zone devices is 1.27 kV, also for a first zone t_p equal to 63 nm, but with second and third zone thicknesses of 57 and 47 nm. Based on the epitaxial structure and measured drift doping concentration, the single-zone design breaks down right at the onset of punch-through, while the triple-zone design can operate well into punch-through. Figure 6(c) shows the breakdown voltage of GaN p-n diodes with single-zone and triple-zone JTE structures as a function of the t_p of single-zone and first zone in the triple-zone case. Triple-zone devices achieve higher V_{br} and reduced sensitivity to t_p. This illustrates the wider fabrication process window and potential to reduce epitaxial p-type growth uniformity requirements (i.e., doping concentration and thickness uniformity).

Temperature-dependent reverse I–V measurements for both the single-zone and triple-zone diodes with a 70 μm diameter were performed from 25 to 75 °C, as shown in Figs. 7(a) and 7(b). A larger increase in reverse current is observed for the single-zone devices compared to triple-zone designs [see the comparison in Fig. 7(b)], indicating the triple-zone design offers higher efficiency at high operation temperatures. To study the mechanism of leakage currents, the current density as a function of the average electric field is plotted in Fig. 7(c). The average electric field is estimated using $E = (V_{bi} - V_r)/W_d$, where V_{bi} is the built-in voltage, V_r is the reverse bias applied, and W_d is the depletion width. The leakage current exhibits a $ln(J) \propto E$ relation over a large reverse bias range. The linear relation between $ln(J)$ and E of the plots [see dashed lines in Fig. 7(c)] suggests an electron

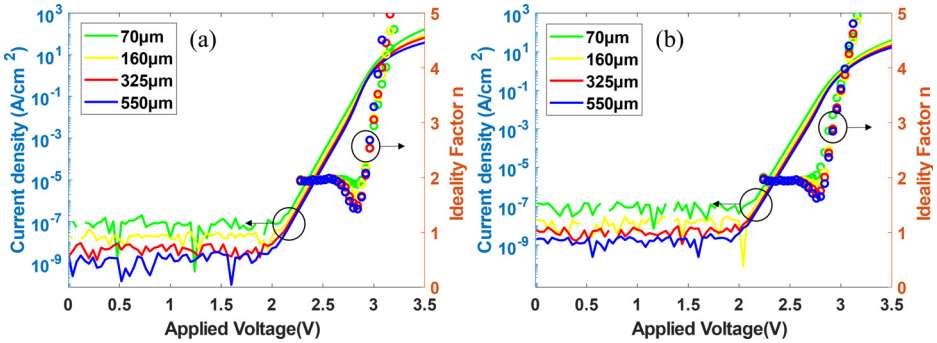

FIG. 5. Measured forward-bias I–V characteristics of the fabricated diodes with diameters from 70 to 550 μm for (a) single-zone and (b) triple-zone JTE structures.

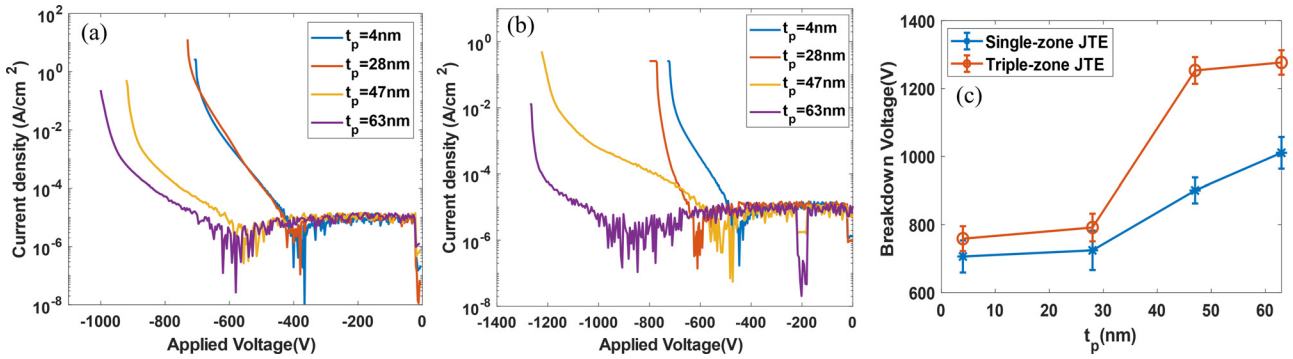

FIG. 6. Measured reverse-bias I–V characteristic of diodes with a diameter of 70 μm at four different t_p for (a) single-zone and (b) triple zone devices. (c) Breakdown voltage of these device as a function of p^- layer thickness (t_p) for both structures. Triple-zone structures improve the process window of t_p.

variable-range-hopping (VRH) mechanism for the triple-zone design.[31–33] The VRH leakage mechanism is expressed by

$$J = J_0 \exp\left(\frac{CE}{2k_B T}\left(\frac{T_0}{T}\right)^{\frac{1}{4}}\right), \tag{1}$$

where T is the temperature, k_B is the Boltzmann constant, J_0 is a pre-exponential factor, C is a constant, and T_0 is the characteristic temperature. Electron hopping along dislocations or through traps is the leakage path under this condition.[32] The single-zone devices present higher leakage currents than the triple-zone devices because the higher peak fields present in the single-zone design [Fig. 4(c)] exacerbate the effect of defects and traps in this design, which is alleviated to some extent by the more gradual field profile possible with the triple-zone approach. The larger reverse leakage current density for small-diameter devices suggests the presence of perimeter leakage current,[34] which could be caused by the high density of defects-induced traps in the ion-implanted GaN.[35,36]

To assess the mechanism governing breakdown, the breakdown voltage vs temperature was measured. An example for a triple-zone device with anode diameter of 70 μm is shown in Fig. 8(a). The measured breakdown voltage increases with increasing temperature, indicating the diode with triple-zone JTE structure achieves avalanche-limited breakdown. The positive temperature coefficient of the breakdown voltage is extracted to be 3×10^{-4}/K according to equation $BV(T) \approx BV_{25^\circ C} \times (1 + \alpha \Delta T)$, in good agreement with values reported previously.[7,8] To assess the stability of the devices, 20 successive reverse I–V measurements of a diode with triple-zone JTE structure were performed to look for any residual trapping or shifts in device performance. As shown in Fig. 8(b), there was no degradation after 20 repetitive measurements up to 1.2 kV.

Vertical GaN p-n diodes with triple-zone JTE structures formed by nitrogen ion-implantation are reported. The proposed triple-zone JTE and conventional single-zone have been compared by simulations and experiments. The triple-zone JTE structure significantly mitigates the electric field crowding at contact and JTE edges due to the graded charge density over the JTE lateral extent. The fabricated triple-zone diodes have demonstrated higher breakdown voltage, lower leakage, and reduced temperature sensitivity of reverse current compared to single-zone structure, with full punch-through and avalanche breakdown achieved. GaN p-n diodes with triple-zone JTE achieve a breakdown voltage of 1.27 kV with R_{on} of 0.6 mΩ cm^2, resulting in a Baliga figure of merit of 2.7 GW/cm^2. The on-resistance in these devices is limited by the p-type Ohmic contact quality ($R_c \sim 5 \times 10^{-4}$ mΩ cm^2). Nevertheless, this level of performance is consistent with prior reports of other avalanche-limited devices with similar drift layer doping and

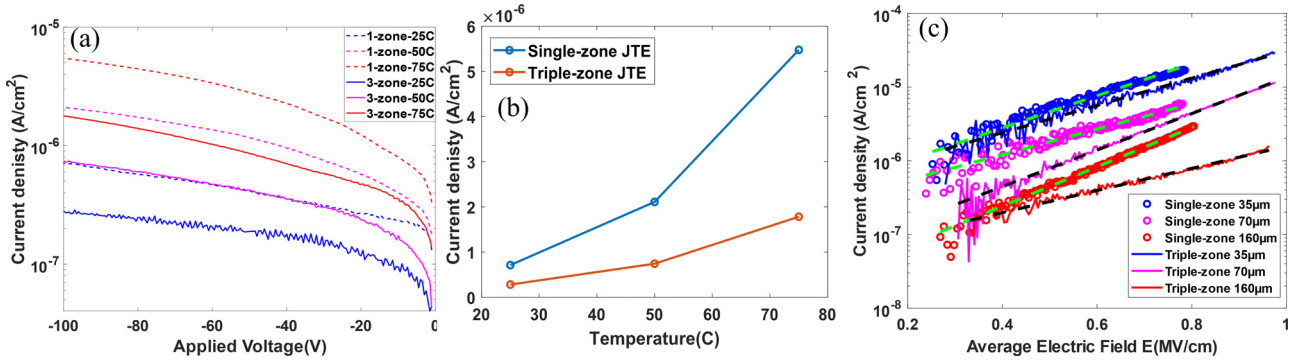

FIG. 7. (a) Measured temperature dependent reverse I–V characteristics of 70 μm diameter diodes. (b) Current density at 100 V bias as a function of temperature, showing the higher leakage and stronger dependence for single-zone compared to three-zone designs. (c) Plot of $ln(J)$ vs average electric field E for diodes with different diameter. The dashed lines show a linear $ln(J)$-E fit suggesting a VRH mechanism. The t_p of single-zone device and first zone of triple-zone device is equal to 63 nm.

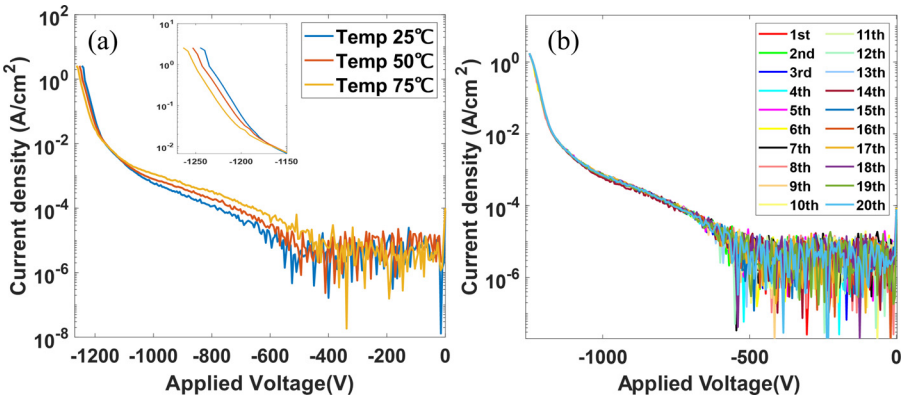

FIG. 8. (a) Temperature dependent reverse I–V characteristics of device with triple-zone JTE, demonstrating positive coefficient of breakdown indicative of an avalanche. (b) Sequential repetitive measurements of reverse I–V characteristics for 20 times, demonstrating the stability of the devices.

thicknesses.[5,11,13,16,19,27] However, a significant benefit of the demonstrated triple-zone JTE configuration is that we obtain a wider fabrication process window for the JTE, as well as a larger margin on epitaxial growth. This significantly improves the fabrication efficiency. The triple-zone JTE provides an effective and reliable method for edge termination in GaN vertical power devices.

This work was supported in part by ARPA-E, Grant No. DE-AR0001008, monitored by Program Manager Isik Kizilyalli.

AUTHOR DECLARATIONS

Conflict of Interest

The authors have no conflicts to disclose.

Author Contributions

Yu Duan: Conceptualization (equal); Formal analysis (equal); Investigation (equal); Methodology (equal); Writing – original draft (equal); Writing – review & editing (equal). **Jingshan Wang:** Resources (equal). **Zhongtao Zhu:** Investigation (supporting). **Guanxi Piao:** Resources (equal). **Kazutada Ikenaga:** Resources (equal). **Hiroki Tokunaga:** Resources (equal). **Shuuichi Koseki:** Resources (equal). **Mayank Bulsara:** Resources (equal). **Patrick J. Fay:** Conceptualization (equal); Funding acquisition (equal); Investigation (equal); Supervision (equal); Writing – review & editing (equal).

DATA AVAILABILITY

The data that support the findings of this study are available from the corresponding author upon reasonable request.

REFERENCES

[1]W. A. Hadi, M. S. Shur, and S. K. O'Leary, J. Mater. Sci.: Mater. Electron. **25**, 4675 (2014).
[2]B. J. Baliga, Semicond. Sci. Technol. **28**, 074011 (2013).
[3]E. P. Carlson, D. W. Cunningham, Y. Z. Xu, and I. C. Kizilyalli, Mater. Sci. Forum **924**, 799 (2018).
[4]F. Roccaforte, P. Fiorenza, G. Greco, R. L. Nigro, F. Giannazzo, A. Patti, and M. Saggio, Phys. Status Solidi A **211**, 2063 (2014).
[5]D. Ji, S. Li, B. Ercan, C. Ren, and S. Chowdhury, IEEE Electron Device Lett. **41**, 264 (2020).
[6]H. Ohta, N. Kaneda, F. Horikiri, Y. Narita, T. Yoshida, T. Mishima, and T. Nakamura, IEEE Electron Device Lett. **36**, 1180 (2015).
[7]K. K. Nomoto, B. Song, Z. Hu, M. Zhu, M. Qi, N. Kaneda, T. Mishima, T. Nakamura, D. Jena, and H. G. Xing, IEEE Electron Device Lett. **37**, 161 (2016).
[8]Z. Bian, K. Zeng, and S. Chowdhury, IEEE Electron Device Lett. **43**, 596 (2022).
[9]H. Fu, K. Fu, X. Huang, H. Chen, I. Baranowski, T. H. Yang, J. Montes, and Y. Zhao, IEEE Electron Device Lett. **39**, 1018 (2018).
[10]C. Yang, H. Fu, K. Fu, T. Yang, J. Zhou, J. Montes, and Y. Zhao, Semicond. Sci. Technol. **36**, 075009 (2021).
[11]W. Lin, M. Wang, R. Yin, J. Wei, C. Wen, B. Xie, Y. Hao, and B. Shen, IEEE Electron Device Lett. **42**, 1124 (2021).
[12]L. Yates, B. P. Gunning, M. H. Crawford, J. Steinfeldt, M. L. Smith, V. M. Abate, J. R. Dickerson, A. M. Armstrong, A. Binder, A. A. Allerman, and R. J. Kaplar, IEEE Trans. Electron Devices **69**, 1931 (2022).
[13]H. Fukushima, S. Usami, M. Ogura, Y. Ando, A. Tanaka, M. Deki, M. Kushimoto, S. Nitta, Y. Honda, and H. Amano, Appl. Phys. Express **12**, 026502 (2019).
[14]H. Ohta, N. Asai, F. Horikiri, Y. Narita, T. Yoshida, and T. Mishima, IEEE Electron Device Lett. **41**, 123 (2020).
[15]T. Maeda, T. Narita, H. Ueda, M. Kanechika, T. Uesugi, T. Kachi, T. Kimoto, M. Horita, and J. Suda, IEEE Electron Device Lett. **40**, 941 (2019).
[16]K. Zeng, S. Chowdhury, B. Gunning, R. Kaplar, and T. Anderson, in *IEEE International Reliability Physics Symposium* (IEEE, 2021), pp. 1–4.
[17]H. Ohta, K. Hayashi, F. Horikiri, M. Yoshino, T. Nakamura, and T. Mishima, Jpn. J. Appl. Phys., Part 1 **57**, 04FG09 (2018).
[18]H. Fu, K. Fu, S. R. Alugubelli, C. Y. Cheng, X. Huang, H. Chen, T. H. Yang, C. Yang, J. Zhou, J. Montes, X. Deng, X. Qi, S. M. Goodnick, F. A. Ponce, and Y. J. Zhao, IEEE Electron Device Lett. **41**, 127 (2020).
[19]V. Talesara, Y. Zhang, Z. Chen, H. Zhao, and W. Lu, J. Mater. Res. **36**, 4919 (2021).
[20]V. A. K. Temple and M. S. Adler, IEEE Trans. Electron Devices **22**, 910 (1975).
[21]R. Pérez, D. Tournier, A. Pérez-Tomás, P. Godignon, N. Mestres, and J. Millán, IEEE Trans. Electron Devices **52**, 2309 (2005).
[22]W. Sung, E. V. Brunt, B. J. Baliga, and A. Q. Huang, IEEE Electron Device Lett. **32**, 880 (2011).
[23]H. Miyake, T. Okuda, H. Niwa, T. Kimoto, and J. Suda, IEEE Electron Device Lett. **33**, 1598 (2012).
[24]T. J. Anderson, B. N. Feigelson, F. J. Kub, M. J. Tadjer, K. D. Hobart, M. A. Mastro, J. K. Hite, and C. R. Eddy, Electron. Lett. **50**, 197 (2014).
[25]J. R. Dickerson, A. A. Allerman, B. N. Bryant, A. J. Fischer, M. P. King, M. W. Moseley, A. M. Armstrong, R. J. Kaplar, I. C. Kizilyalli, O. Aktas, and J. J. Wierer, IEEE Trans. Electron Devices **63**, 419 (2016).
[26]J. Wang, L. Cao, J. Xie, E. Beam, R. McCarthy, C. Youtsey, and P. Fay, Appl. Phys. Lett. **113**, 023502 (2018).
[27]Y. Cao, J. W. Pomeroy, M. J. Uren, F. Yang, J. Wang, P. Fay, and M. Kuball, Appl. Phys. Lett. **120**, 242106 (2022).
[28]J. Wang, R. McCarthy, C. Youtsey, R. Reddy, J. Xie, E. Beam, L. Guido, L. Cao, and P. Fay, Phys. Status Solidi A **216**, 1800652 (2019).

[29]See http://www.srim.org. for "SRIM-2013," 2013.
[30]See https://www.synopsys.com for "Synopsys Sentaurus 2015," 2015.
[31]D.-P. Han, C.-H. Oh, H. Kim, J.-I. Shim, K.-S. Kim, and D.-S. Shin, IEEE Trans. Electron Devices **62**, 587 (2014).
[32]Y. Zhang, H.-Y. Wong, M. Sun, S. Joglekar, L. Yu, N. A. Braga, R. V. Mickevicius, and T. Palacios, in *IEEE International Electron Devices Meeting* (IEEE, Washington, 2015), p.35.1.1.
[33]X. Guo, Y. Zhong, X. Chen, Y. Zhou, S. Su, S. Yan, J. Liu, X. Sun, Q. Sun, and H. Yang, Appl. Phys. Lett. **118**, 243501 (2021).
[34]Y. Zhang, M. Sun, H.-Y. Wong, Y. Lin, P. Srivastava, C. Hatem, M. Azize, D. Piedra, L. Yu, T. Sumitomo, N. A. Braga, and T. Palacios, IEEE Trans. Electron Devices **62**, 2155 (2015).
[35]A. M. Ozbek and B. J. Baliga, IEEE Electron Device Lett. **32**, 300 (2011).
[36]D. Alok, B. J. Baliga, and P. K. McLarty, IEEE Electron Device Lett. **15**, 394 (1994).